Proceedings of the 10th Brazilian Congress of Thermal Sciences and Engineering – ENCIT 2004
Braz. Soc. of Mechanical Sciences and Engineering – ABCM, Rio de Janeiro, Brazil, Nov. 29 – Dec. 03, 2004

Paper CIT04-0733

DISPLACEMENT OF DILUTE POLYMER SOLUTIONS IN CAPILLARY TUBES

Erick Fabrízio Quintella
PUC-Rio, Departament of Mechanical Engineering
Rua Marquês de São Vicente 225, Rio de Janeiro, RJ, Brazil
erick@mec.puc-rio.br

Paulo Roberto de Souza Mendes
PUC-Rio, Departament of Mechanical Engineering
Rua Marquês de São Vicente 225, Rio de Janeiro, RJ, Brazil
pmendes@mec.puc-rio.br

Márcio da Silveira Carvalho
PUC-Rio, Departament of Mechanical Engineering
Rua Marquês de São Vicente 225, Rio de Janeiro, RJ, Brazil
msc@mec.puc-rio.br

Abstract. *Displacement of a liquid in a capillary tube by gas injection occurs in many situations, like enhanced oil recovery, coating of catalytic converters and gas-assisted injection molding. Generally the liquid being displaced is a polymeric solution or dispersion, which is not Newtonian. Viscoelastic forces alter the force balance in various parts of the flow and consequently change the amount of liquid left attached to the capillary wall. Models of such flows must rely on theories that can account for the different behavior of microstructured liquids in shear and extensional flow. Moreover, displacement flows involve a free surface, and the domain where the differential equations are posed is unknown a priori being part of the solution. These two characteristics make the problem extremely complex. Here, the two-dimensional free surface flow near the gas-liquid interface was modelled using three different differential constitutive equations that approximate viscoelastic behavior of dilute polymer solutions, namely Oldroyd-B, FENE-P and FENE-CR, together with momentum and continuity equations. The equation system was solved with the Finite Element Method. The resulting non-linear system of algebraic equations was solved by Newton's method. The results show the effect of the viscoelastic character of the liquid on the free surface configuration and the film thickness attached to the capillary wall.*

keywords: *Free surface flow, two-phase viscoelastic flow, gas-assisted injection molding, gas-liquid interface, elastic dumbbell models.*

1. Introduction

The displacement of a liquid inside small passages and capillary tubes by another liquid or gas occurs in many practical situations. The most important examples are the flow inside the porous space in enhanced oil recovery methods, coating process of catalytic converter and inside tubes and gas assisted injection molding. These flows belong to a class of flows generally referred to as free surface flows; the configuration and position of the interface between the two fluids is unknown a priori and it is part of the solution of the problem.

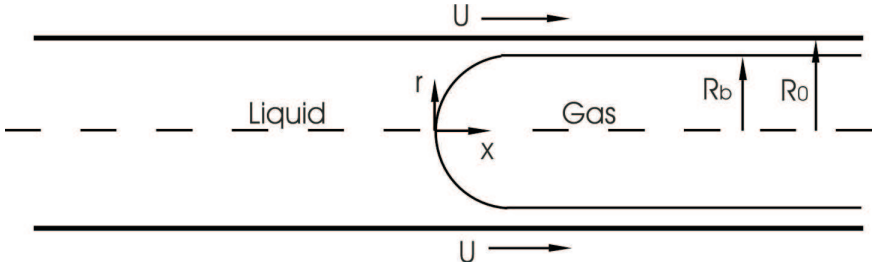

Figure 1: Sketch of a liquid-displacement problem.

Figure (1) shows the region close to the tip of the interface of a liquid being displaced by a gas. Since the frame of reference is attached to the bubble tip, all happens as if the tube wall is moving with the bubble speed U in the opposite direction. A certain amount of liquid remains attached to the capillary wall, as shown in the figure. The more liquid is left on the wall the least efficient is the displacement process. This information is one of the main goals of theoretical and experimental analysis of displacement flows.

A dimensionless measurement of the thickness of the liquid film attached to the wall used in the literature is the fractional coverage m, defined as the fraction of the tube cross-sectional area coated with liquid after bubble penetration, i.e.

$$m = 1 - \frac{R_b^2}{R_0^2}, \tag{1}$$

where R_0 is the tube radius and R_b is the radius of the penetrating bubble. In some of the situations described, the liquid being displaced is a polymeric solution or dispersion and is not Newtonian. Viscoelastic forces near the interface changes the force balance in that region and consequently the configuration of the free surface and the fractional coverage. The two important dimensionless groups in the displacement of viscoelastic liquids in capillary tubes, our case of interest, are the capillary number Ca, which is the ratio of viscous to surface tension forces, and the Weissenberg number We, which is the ratio between a relaxation time characteristic of the liquid and a characteristic time of the deformation process:

$$Ca = \frac{\eta U}{\sigma}, \qquad We = \lambda \dot{\gamma}_w. \tag{2}$$

Here η is the total viscosity of the liquid phase, U is the bubble velocity, σ is the interfacial tension between the inviscid penetrating gas and the displaced liquid, λ is a relaxation time characteristic of the liquid and $\dot{\gamma}_w = 2U/R_0$ is the (Newtonian) shear rate at the wall, assumed to be characteristic of the process.

Different analyses on displacement of liquids in capillary tubes have been performed for Newtonian as well as for viscoelastic liquids, and a brief summary of these results is given in the following paragraphs.

The first experimental study of a long gas bubble penetrating through a liquid in a capillary tube was performed by Fairbrother and Stubbs, 1935. Their most important result is the proposition of a direct relation between the fractional coverage m with the capillary number Ca, given by $m = Ca^{\frac{1}{2}}$.

The first theoretical analysis on liquid displacement in capillary tubes was developed by Bretherton, 1961. He studied the motion of long air bubbles in capillary tubes filled with Newtonian viscous liquids. Bretherton assumed zero shear stress at the interface, as well as small capillary numbers. Bretherton performed experimental tests with tubes of diameters small enough to neglect gravity effects. His theoretical analysis showed a relation of the thin film thickness attached at the wall with the capillary number as $m \approx 1.29(3Ca)^{\frac{2}{3}}$.

Taylor, 1961 developed an experimental study on removal of Newtonian liquids from capillary tubes through gas injection. The main objective was to determine the amount of liquid deposited on the tube wall during flow. Taylor showed the dependence of the fractional coverage m, with the capillary number, Ca. The plot suggests a limit value for m corresponding to approximately 0.56 when Ca tends to 2. Fairbrother and Stubbs had already proposed a direct relation of m with the capillary number, as mentioned. Taylor compared his experimental results with the empirical equation proposed by Fairbrother and Stubbs and verified that their relation is only valid for a narrow capillary number range of $0 < Ca < 0.09$.

One year later, Cox, 1962 published the continuation of the experiments initiated by Taylor and concluded that the fraction of mass deposited at the wall reaches an asymptotic value of 0.60 when Ca tends to 10. Cox also developed a simplified theoretical analysis to calculate m. His analysis appears to fit in the cases where surface tension forces can be neglected in view of viscous forces ($Ca >> 1$).

Regarding the displacement of viscoelastic liquids, Ro and Homsy, 1995 presented a theoretical study about the effect of elasticity on the meniscus shape and on film thickness for the flow induced by a long air bubble steadily displacing a polymeric liquid confined by two parallel plates, i.e. Hele-Shaw flow. The authors sought asymptotic solutions by perturbation expansions to solve the problem, and the assumptions were that the displaced viscoelastic liquid wets the wall and that both capillary number and local Weissenberg number were small. The Oldroyd-B constitutive equation was used to model the viscoelastic liquid and the authors stressed that the transition region between the advancing meniscus and the entrained film is where the liquid rheology has its greatest effect. A detailed analysis of their work allows concluding that the main mechanisms in this flow are the resistance to stream-wise strain, tending to lower the film thickness, and the buildup of shear stress, tending to raise the film thickness. According to their analysis, in the limit of small Ca and We, as the liquid becomes more viscoelastic, the film thickness decreases, implying that the stream-wise resistance is the dominant mechanism at this range.

Huzyak and Koelling, 1997 performed experimental investigations of penetration of a long bubble through a viscoelastic liquid in a capillary tube. The main goal was to identify the effects of liquid elasticity on the

thickness of the liquid film attached to the wall. Experiments were performed with four test liquids including two Newtonian and two Boger liquids (highly elastic liquids showing constant shear viscosities). The authors obtained results for the fractional coverage m, as a function of capillary number and Deborah number, De. Deborah number, like Weissenberg number, measures the deviation of elastic fluids from Newtonian behavior.

The authors concluded that for small Deborah number, $De < 1$, both viscoelastic liquids exhibit a fractional coverage identical to that of a Newtonian liquid at an equivalent capillary number. Nevertheless, depending on ones estimate of the experimental accuracy, fluid thickness at this De range presents a slight thinning of the film. The fractional coverage for both viscoelastic liquids begins to increase relative to the Newtonian result at $De \approx 1$. Fractional coverage continues to increase with Deborah number for all $De \geq 1$. At $De \approx 5$ fractional coverage is 30% greater than the Newtonian liquid result. They also found that the fractional coverage depend on the tube diameter for the viscoelastic liquids.

Another important study dealing with viscoelastic free surface flows was recently presented by A. G. Lee and Khomami, 2002. They applied a finite element formulation to study the effect of viscoelasticity on free surface flows, analyzing both a Hele-Shaw flow and the slot coating of viscoelastic liquids. The viscoelastic liquids were modeled by means of three distinct differential constitutive equations: the Oldroyd-B, FENE-CR and FENE-P models. The calculation showed the formation of an elastic stress boundary layer in the region adjacent to the interface, and the polymeric stresses associated to this boundary layer are found to be responsible for changing the meniscus shape in order to increase the thickness of the liquid attached to the solid plates.

The goal of this work is to analyze the effect of the viscoelastic character of the displaced liquid on the free surface shape and on the film thickness attached to the capillary wall, by solving the momentum and continuity equations coupled with the Oldroyd-B, FENE-P and FENE-CR models to describe the mechanical behavior of the flowing liquid.

2. Mathematical Formulation

2.1. Governing equations

The two-dimensional, steady free surface flow of the displaced liquid in a capillary tube is described by the conservation of mass and momentum equations:

$$\nabla \cdot \mathbf{u} = 0 \tag{3}$$

$$0 = -\nabla p + \nabla \cdot \boldsymbol{\tau} \tag{4}$$

where $\mathbf{u}$ is the velocity vector, p is the pressure and $\boldsymbol{\tau}$ is the extra-stress tensor. It is clear from Eq.(4) that inertial effects are neglected in our model. The governing equations are solved by considering a coordinate system attached to the bubble tip.

2.2. Constitutive equations

The viscoelastic liquid is assumed to be a dilute solution of a high molecular weight polymer. The solvent is taken to be a Newtonian fluid with viscosity η_s.

The extra-stress tensor of the polymer solution can be written as the sum of a contribution from the Newtonian solvent and from the polymer,

$$\boldsymbol{\tau} = \boldsymbol{\tau}_s + \boldsymbol{\tau}_p = \eta_s \dot{\boldsymbol{\gamma}} + \boldsymbol{\tau}_p. \tag{5}$$

Here, η_s is the solvent viscosity and $\dot{\boldsymbol{\gamma}} = \nabla \mathbf{u} + \nabla \mathbf{u}^T$ is the rate of deformation tensor.

We idealize the polymer molecule as an elastic dumbbell, that is, two beads connected by a spring. The beads represent molecular segments of several monomers and the spring describes the entropic effects to which the end-to-end vector of the polymer is subject. There are many kinds of elastic dumbbell models depending on the choice of the spring force law.

Next, we summarize the expressions for the three chosen models: Oldroyd-B, FENE-P and FENE-CR (details can be found in R. B. Bird and Hassager, 1987a and R. B. Bird and Hassager, 1987b).

2.2.1. Elastic dumbbell models

The models used to describe the evolution of the polymeric stress were:

- Oldroyd-B model

$$\boldsymbol{\tau}_p + \lambda_H \boldsymbol{\tau}_{p(1)} = \eta_p \dot{\boldsymbol{\gamma}}. \tag{6}$$

- FENE-P model

$$Z\boldsymbol{\tau}_p + \lambda_H \boldsymbol{\tau}_{p(1)} - \lambda_H \left[\boldsymbol{\tau}_p + \left(\frac{\eta_p}{\lambda_H}\right)\mathbf{I}\right]\frac{D}{Dt}(\ln Z) = \eta_p \dot{\boldsymbol{\gamma}}, \tag{7}$$

where

$$Z = 1 + \frac{3}{b}\left[1 + \left(\frac{\lambda_H}{3\eta_p}\right)\text{tr }\boldsymbol{\tau}_p\right]. \tag{8}$$

- FENE-CR model

$$Z\boldsymbol{\tau}_p + \lambda_H \boldsymbol{\tau}_{p(1)} - \lambda_H \boldsymbol{\tau}_p \frac{D}{Dt}(\ln Z) = Z\eta_p \dot{\boldsymbol{\gamma}}, \tag{9}$$

where

$$Z = \frac{1 + (\lambda_H / b\eta_p)\text{tr }\boldsymbol{\tau}_p}{1 - (3/b)}. \tag{10}$$

The Oldroyd-B model is a Hookean dumbbell model, i.e., the tension in the spring is proportional to the bead separation. Here, λ_H is the time constant for the Hookean dumbbells, η_p is the polymer contribution to the shear viscosity and the subscrit $_{(1)}$ denotes the upper-convected differentiation operator. The Oldroyd-B model gives steady-state shear flow material functions that are independent of the shear rate and also a steady-state elongational viscosity that goes to infinity at a finite elongation rate; this unlikely behavior results because the linear spring model allows infinite extension.

The linear (Hookean) spring force is realistic only for small deformations from equilibrium and puts no limit to the extent to which the dumbbell can be stretched. An approach which corrects this unphysical behavior and seems to play important role in non-linear rheological phenomena is the idea of finite extensibility. Dumbbell models with finite extensible non-linear elastic (FENE) spring forces are widely used in numerical flow calculations.

The FENE-P model is a non-Hookean dumbbell model, i.e., the tension in the spring is a non-linear function of the bead separation. Here, λ_H is the same time constant defined for Hookean dumbbells and η_p is the polymer contribution to the shear viscosity. b is a dimensionless parameter which measures the finite extensibility. Note that as b approaches infinity, the Oldroyd-B model is recovered. The steady-state shear flow material functions in the FENE-P model are a function of the shear rate. Then, the FENE-P model is a better choice for computations of shear-thinning viscoelastic liquids.

The FENE-CR model is also a non-Hookean dumbbell model. Its parameters are the same as in the FENE-P model, and it also recovers the Oldroyd-B model as b approaches infinity. The main difference is that this model was designed to eliminate the shear rate dependence of the steady state viscosity, becoming, then, a suitable model to describe Boger fluids.

2.3. Boundary conditions

The boundary conditions applied on the free surface are:

- Kinematic condition

$$\mathbf{n} \cdot \mathbf{u} = 0; \tag{11}$$

- Force balance

$$\mathbf{n} \cdot (\boldsymbol{\tau} - p\mathbf{I}) = \frac{\sigma}{R_m}\mathbf{n}. \tag{12}$$

Additional boundary conditions are stated below:

- Non-slip condition on the tube wall

$$\mathbf{u} = U\mathbf{e}_x; \tag{13}$$

- Symmetry condition at the centerline

$$\mathbf{n} \cdot \mathbf{u} = 0, \ \mathbf{t} \cdot \mathbf{T} \cdot \mathbf{n} = 0; \tag{14}$$

- Fully developed flow with pressure free at the outflow

$$\mathbf{n} \cdot \nabla \mathbf{u} = 0; \tag{15}$$

- Fully developed flow with pressure imposed at the inflow

$$\mathbf{n} \cdot \nabla \mathbf{u} = 0, \ p = P_0. \tag{16}$$

In these equations, $\mathbf{n}$ and $\mathbf{t}$ are the unit vectors normal and tangent to the domain boundary, respectively. $\mathbf{T}$ is the total stress tensor, $\mathbf{e}_x$ is the unit vector in the axial direction, U is the velocity at the tube wall, P_0 is the imposed pressure at the inflow, σ is the surface tension and R_m is the local mean radius of curvature of the interface.

3. Solution Method

A finite element method is applied to study this viscoelastic free surface flow. The formulation implemented is the DEVSS-G/SUPG formulation proposed by Guenette and Fortin, 1995 and Brooks and Hughes, 1982.

3.1. Free surface parametrization

The relevant differential equations are posed in an unknown domain; the position of the liquid free surface is part of the solution. A simple way of solving this type of problem is to use a Picard iteration, i.e. solve the flow and the domain position separately. This procedure is not very efficient and in most cases the iteration does not converge. To compute a free boundary problem in a more efficient way, the set of differential equations posed in the unknown physical domain has to be transformed to an equivalent set defined in a known reference domain, usually called computational domain. This transformation is made by a mapping $\mathbf{x} = \mathbf{x}(\boldsymbol{\xi})$ that connects the two domains. The inverse of the mapping that minimizes the functional is governed by elliptic differential equations identical to those encountered in diffusion transport with variable diffusion coefficients. The coordinates of the reference domain satisfy

$$\nabla \cdot (\boldsymbol{D} \cdot \nabla \boldsymbol{\xi}) = 0, \tag{17}$$

where $\boldsymbol{D}$ is the diffusion coefficient tensor and $\boldsymbol{\xi}$ are the coordinates of the reference domain.

Boundary conditions are needed to solve these second-order partial differential equations. Along solid walls and synthetic inlet and outlet planes, the boundary is located by imposing a relation between the physical coordinates x and r from the equation that describes the shape of the boundary, and stretching functions are used to distribute the points along the boundaries. The free boundary (gas-liquid interface) is located by imposing the kinematic condition (Eq.(11)). The discrete versions of the mapping equations are generally referred to as mesh generation equations.

3.2. Interpolation functions

The unknown fields are written as a linear combination of polynomial basis functions. Thus, the velocity vector $\mathbf{u}$, pressure p, nodal position vector $\mathbf{x}$, interpolated velocity gradient tensor $\mathbf{g}$ and polymeric stress tensor $\boldsymbol{\tau}_p$ are approximated by, respectively:

$$\mathbf{u} = \sum_{j=1}^{9}(\mathbf{U}_j\phi_j), p = \sum_{j=1}^{3}(P_j\chi_j), \mathbf{x} = \sum_{j=1}^{9}(\mathbf{X}_j\phi_j), \mathbf{g} = \sum_{j=1}^{4}(\mathbf{G}_j\psi_j), \boldsymbol{\tau}_p = \sum_{j=1}^{4}(\mathbf{I}_{p_j}\psi_j). \tag{18}$$

Here, $\mathbf{U}_j$, P_j, $\mathbf{X}_j$, $\mathbf{G}_j$, $\mathbf{I}_{p_j}$ are the basis functions coefficients, and represent the unknowns of the discretized problem. The basis functions $\phi_j(\xi, \eta)$ are biquadratic, $\chi_j(\xi, \eta)$ are linear discontinuous and $\psi_j(\xi, \eta)$ are bilinear.

3.3. Weak formulation of the governing equations in the reference domain

The conservation of mass, conservation of linear momentum, interpolated velocity gradient and mesh generation equations are solved using the Galerkin method. For their hyperbolic nature, all three differential constitutive equations are solved using the Petrov-Galerkin streamline upwinding method (SUPG). The weak forms of the governing equations are, in tensor notation:

- Conservation of mass

$$R_c = \int_\Omega (\nabla \cdot \mathbf{u}) \chi J d\Omega \tag{19}$$

- Conservation of linear momentum

$$R_m = \int_\Omega \mathrm{tr}(\mathbf{T} \cdot \nabla \mathbf{w}) J d\Omega - \int_\Gamma (\mathbf{n} \cdot \mathbf{T}) \cdot \mathbf{w} J d\Gamma \tag{20}$$

- Interpolated velocity gradient

$$R_g = \int_\Omega (\mathbf{g} - \nabla \mathbf{u} + \frac{\nabla \cdot \mathbf{u}}{\mathrm{tr}\ \mathbf{I}} \mathbf{I}) : \boldsymbol{\psi} J d\Omega \tag{21}$$

- Mesh generation

$$R_X = -\int_\Omega (\nabla \mathbf{w} : \boldsymbol{D} \cdot \nabla \boldsymbol{\xi}) J d\Omega + \int_\Gamma (\mathbf{n} \cdot \boldsymbol{D} \cdot \nabla \boldsymbol{\xi}) \cdot \mathbf{w} d\Gamma \tag{22}$$

- Oldroyd-B model

$$R_{\boldsymbol{\tau}_p} = \int_\Omega (\boldsymbol{\tau}_p + \lambda_H \boldsymbol{\tau}_{p(1)} - \eta_p \dot{\boldsymbol{\gamma}}) : \boldsymbol{\varphi} J d\Omega \tag{23}$$

- FENE-P model

$$R_{\boldsymbol{\tau}_p} = \int_\Omega \left\{ Z \boldsymbol{\tau}_p + \lambda_H \boldsymbol{\tau}_{p(1)} - \lambda_H \left[\boldsymbol{\tau}_p + \left(\frac{\eta_p}{\lambda_H} \right) \mathbf{I} \right] \frac{D}{Dt} (\ln Z) - \eta_p \dot{\boldsymbol{\gamma}} \right\} : \boldsymbol{\varphi} J d\Omega \tag{24}$$

- FENE-CR model

$$R_{\boldsymbol{\tau}_p} = \int_\Omega \left\{ Z \boldsymbol{\tau}_p + \lambda_H \boldsymbol{\tau}_{p(1)} - \lambda_H \boldsymbol{\tau}_p \frac{D}{Dt} (\ln Z) - Z \eta_p \dot{\boldsymbol{\gamma}} \right\} : \boldsymbol{\varphi} J d\Omega \tag{25}$$

Here, Ω and Γ denote the reference domain and its boundary, respectively. J is the Jacobian of the mapping between the physical and reference domain, χ is the scalar weighting function for the conservation of mass equation, $\mathbf{w}$ is the vector weighting function for the conservation of momentum and mesh generation equations, $\boldsymbol{\psi}$ is the tensor weighting function for the interpolated velocity gradient, $\boldsymbol{\varphi}$ is the tensor weighting function for the constitutive equations and $\mathbf{I}$ is the unit tensor.

3.4. Solution of the problem via Newton iterations

The resulting nonlinear system of equations is solved by the Newton's method:

$$\mathbf{J} \cdot \delta \mathbf{c} = -\mathbf{R}(\mathbf{c}), \tag{26}$$

$$\mathbf{c}^{k+1} = \mathbf{c}^k + \delta \mathbf{c}. \tag{27}$$

$\mathbf{J}$ is the Jacobian matrix containing the derivatives of all equations with respect to all unknowns, $\mathbf{c}$ is the solution vector containing all the unknowns of the problem, $\delta \mathbf{c}$ is the increment in the solution vector, $\mathbf{R}$ is a vector of weighted residuals and k indicates the present iteration.

4. RESULTS

4.1. Newtonian results

Before presenting the analysis of the displacement of viscoelastic liquids in capillary tubes, some classical results for Newtonian liquids are presented in order to test the solution procedure, provide basic information on the subject and gain insight for more complex analysis later.

Figure (2) shows the dependence of the liquid film thickness deposited at the tube wall on the capillary number. Simulations cover a capillary number range of $0.01 \leq Ca \leq 10$. Besides theoretical predictions obtained in the present work, we reproduce the experimental data obtained by Taylor, 1961. The agreement between both results is excellent. The result obtained by Cox, 1962, which suggests a constant value of 0.6 to the fractional coverage for capillary number above 10, is also confirmed. The experimental results obtained by Taylor, as well as the theoretical predictions of the present work, show that for a given viscosity and a given surface tension the film thickness deposited at the wall is controlled by the velocity of the interface. Therefore, processes whose objective is to obtain a thin film thickness must be performed at low flow rates.

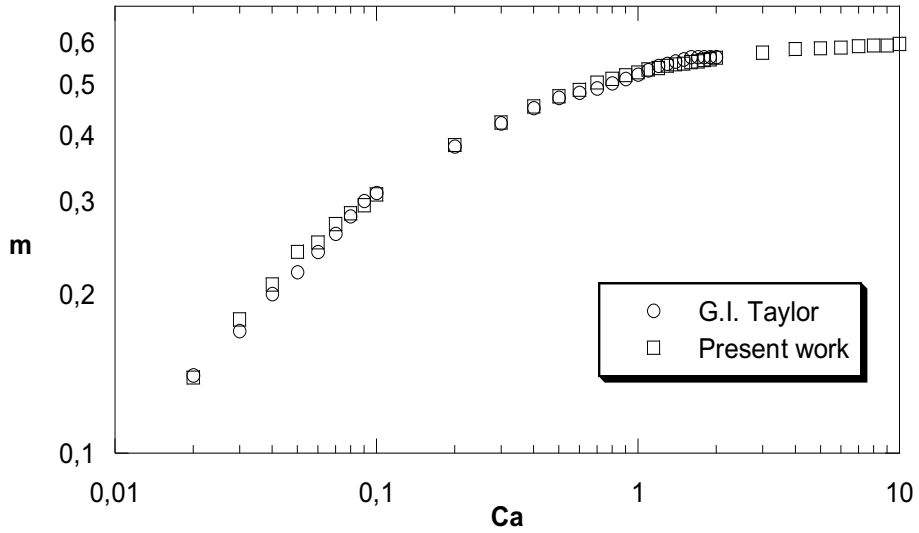

Figure 2: Newtonian liquid film thickness as a function of Ca.

4.2. Viscoelastic Effect

When polymer additives are incorporated to the Newtonian liquid the force balance in the different regions of the flow changes. The elastic character of the polymer molecules is displayed by the appearance of elastic stresses at regions of high flow straining, mainly close to the free surface. To reach a new equilibrium configuration, the free surface curvature is changed and, consequently, the amount of liquid attached to the capillary wall is also changed.

In order to study solely the viscoelastic effects on film thickness, we follow Huzyak and Koelling, 1997 suggestion of plotting a reduced fractional coverage against Weissenberg numbers. Reduced fractional coverage is defined as the ratio between the liquid film thickness obtained with a viscoelastic liquid (m) to that obtained with a Newtonian liquid at the same capillary number (m_N). Figure (3) shows the theoretical predictions for an Oldroyd-B liquid of reduced fractional coverage plotted against Weissenberg number. The results are at $Ca = 0.1$. Although the flow states shown are at a particular Ca and Oldroyd-B is the single model used, computations in all capillary numbers analyzed with all models present qualitatively similar results.

The results shown in Fig.(3) agree qualitatively with experimental data reported in the literature (Huzyak and Koelling, 1997, for example). At small Weissenberg numbers, the viscoelastic behavior of the flowing liquid causes a reduction of fluid film thickness with respect to the Newtonian case, and at large Weissenberg number, the film thickness rises as the liquid becomes more elastic.

The effect of variation in the extensibility parameter b on the film thickness for a particular capillary number, $Ca = 0.1$, is shown in Fig.(4). Comparisons are made for FENE-CR model in Fig.(4a) and FENE-P model in Fig.(4b). We follow Herrchen and Ottinger, 1997 recommendation, who use extensibility parameter values $b = 20, 50, 100$, arguing that 20 is at the lower physically meaningful limit and values larger than 100 cause only minor modifications of the Hookean dumbbell (or Oldroyd-B) model. Oldroyd-B results are plotted in

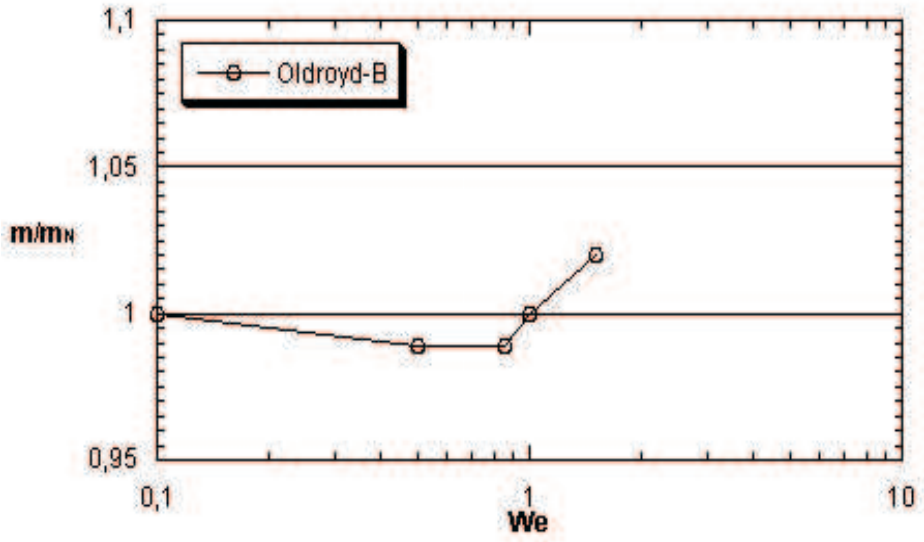

Figure 3: Oldroyd-B reduced fractional coverage m/m_N as a function of We for $Ca = 0.1$.

both comparisons to establish the superior limit for molecule extensibility. Since convergence are compromised with molecule extensibility, simulations for the infinitely extensible molecule based model, Oldroyd-B, could not advance beyond $We = 1.5$.

For small Weissenberg numbers both models present a film thinning, related to the Newtonian case, for any value of extensibility parameter, b. This result suggests that, at this level of elasticity, the adverse stretching stress gradient that causes the film thinning, as shown by A. G. Lee and Khomami, 2002, imposes the same effect on both shear-thinning liquids (FENE-P) and Boger liquids (FENE-CR).

Differences in model behavior appear at higher Weissenberg numbers. Predictions with the FENE-CR model with flexible polymer molecules ($b = 100$) present a film thickening for increasing We, but reaches a plateau at $We \geq 4.0$. Predictions with semi-flexible polymer molecules ($b = 50$) also show film thickenning for increasing We and also reaches a plateau at $We \geq 2.5$. The rigid polymer molecule results ($b = 20$) follow a different trend. Fluid film thickening at this level of We is related to the onset of a stress boundary layer over the free surface, as concluded by A. G. Lee and Khomami, 2002, and the thickness plateau suggests that a maximum value of the stretching polymeric stress tensor component over the free surface is reached.

Results for flexible polymer molecule and rigid polymer molecule FENE-P solutions are qualitatively similar to their FENE-CR correspondent. But instead of presenting a thickening behavior for increasing Weissenberg numbers, FENE-P solution with semi-flexible polymer molecules maintains its constant thinner behavior related to the Newtonian case.

Our simulation of flexible polymer molecule solutions agrees with experimental observations produced by D. Bonn and Meunier, 1995, who observed large film thickening for flexible polymer solutions. On the other hand, our observation of a thinner and thinner behavior for rigid polymer molecule solutions disagrees with Bonn et al. observations, who detected a small film thickening even for more rigid polymer solutions. It is important to mention that this comparison is only qualitative, because our case of study is the axisymmetric counterpart of planar Bonn et al. case of study and the extensibility parameters in our simulations do not represent accurately the molecule flexibilities of Bonn et al. experimental solutions.

4.2.1. Fitting experimental data

Huzyak and Koelling, 1997 performed experiments to investigate the penetration of a long bubble through a viscoelastic liquid in a capillary tube. In their work, the results were presented for four test fluids with rheological properties designed such that the effects of liquid elasticity could be isolated from shear thinning phenomena (Boger fluids). In order to perform a comparison between their experimental data with our theoretical predictions, Fig.(5) shows the fractional coverage as a function of capillary number. The experimental data corresponding to one of the viscoelastic liquids developed by Huzyak and Koelling (B-35) is compared with our theoretical predictions. The rheological data for fluid B-35 in Huzyak and Koelling, 1997 was fitted to a FENE-CR model, chosen for being suited to fit Boger fluid data. The relevant parameters turned to be $\eta_s + \eta_p = 2.90$ Pa.s, $b = 658$ and $\lambda = 0.28$ s. Since a value of b above 100 implies only minor modifications on the Hookean spring behavior, we should expect the present results to be very similar when obtained with an Oldroyd-B model. Since Huzyak and Koelling sustain that fractional coverage values depend on tube radii, the

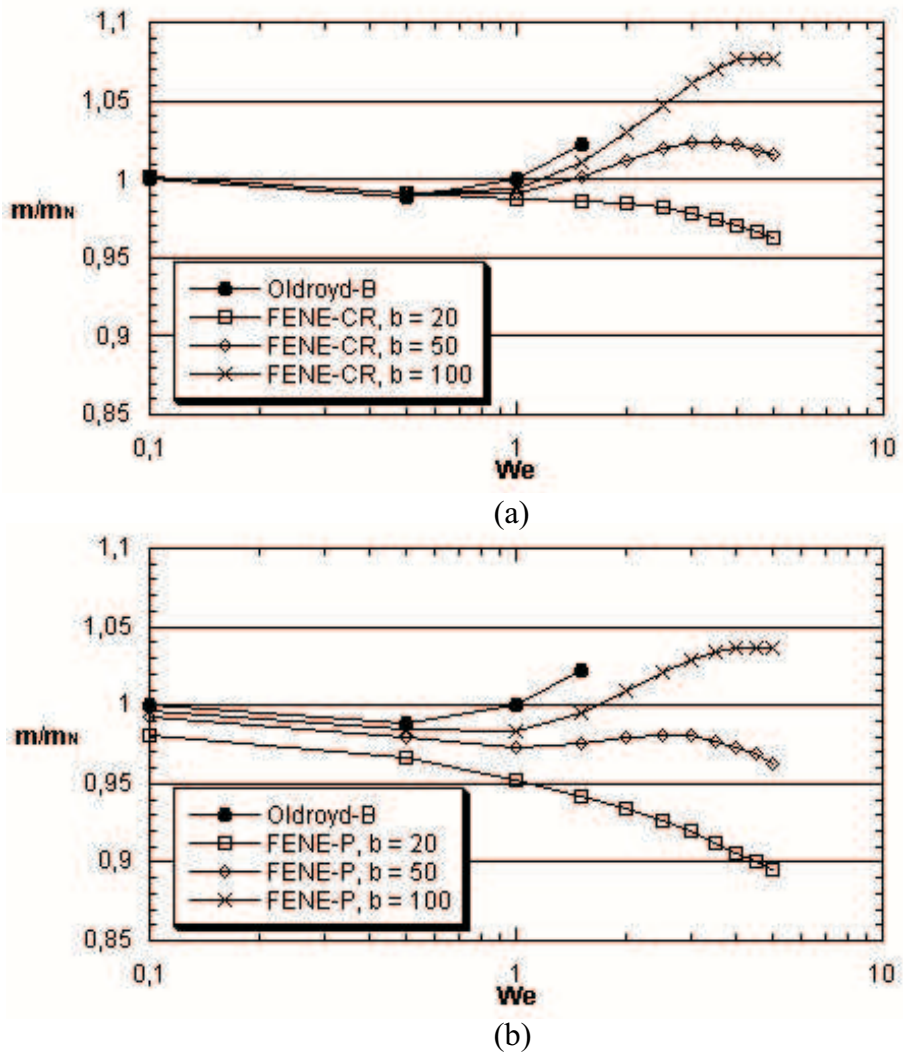

Figure 4: Molecule extensibility parameter variation effects on film thickness. Results are for $Ca = 0.1$. (a) FENE-CR model; (b) FENE-P model.

presented numerical simulations were performed at the same tube radius used for the B-35 fluid experiments, i.e., $R_0 = 0.246$ cm. Fractional coverage for the Newtonian fluid is included in this plot as a reference.

The agreement between Huzyak and Koelling experimental results and the theoretical predictions reported here is good. Since the elasticity of Boger fluids should not be important at low shear rates, both experimental e theoretical data are nearly the same as the Newtonian fluid data for $Ca < 1$. However, at capillary numbers above 1 a significative deviation is noted from Newtonian behavior. The experimental results show a fractional coverage of $m = 0.663$ (12% greater than the corresponding Newtonian result) at $Ca = 5$, while our theoretical results predict a fractional coverage of $m = 0.702$ (17% greater than the corresponding Newtonian result) for the same capillary number. Another important observation is that although the Newtonian results show an asymptotic behavior tending to a value of $m = 0.600$ with increasing capillary numbers, both experimental and theoretical viscoelastic data continue to increase with capillary number .

5. Final Remarks

A two dimensional viscoelastic flow near the gas-liquid interface of a long bubble displacing a liquid in a capillary tube was presented. The presence of the free surface, that makes the domain of integration unknown a priori, and the differential constitutive models needed to describe the behavior of dilute polymeric solutions make the solution of the problem extremely complex. A fully coupled formulation was used and the differential equations were solved by the Finite Element Method.

The results show that viscoelastic forces tend to decrease the amount of liquid left attached to the tube wall for small values of Weissenberg numbers and to increase the fluid film thickness at high Weissenberg number, a

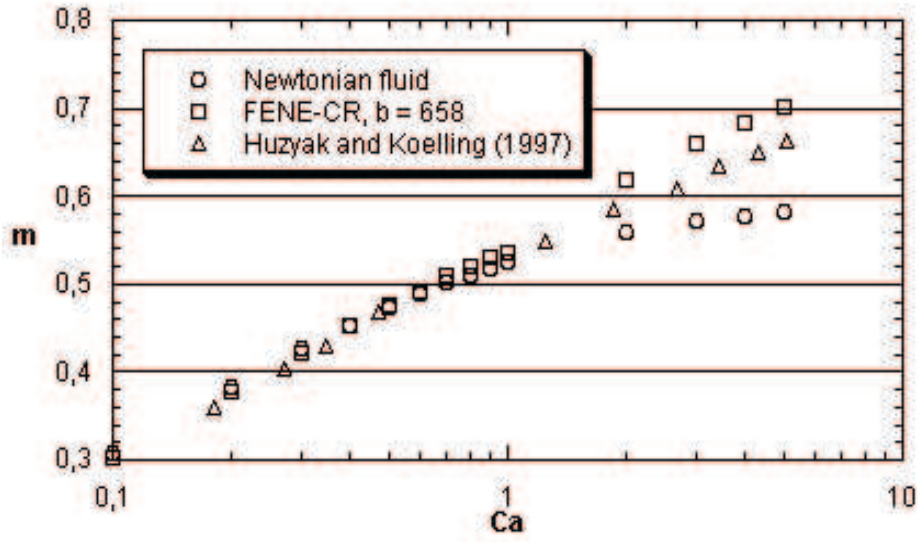

Figure 5: Fractional coverage as a function of capillary number for Newtonian fluids, for the FENE-CR model with $\eta_s + \eta_p = 2.90$, $b = 658$ and $\lambda = 0.28$ s and for fluid B-35 from (Huzyak and Koelling, 1997).

trend observed experimentally by other researchers. The results also show that for the non-linear spring model, the film thickness on the wall reaches a maximum value, probably associated with the maximum normal stress along the streamlines.

6. Acknowledgements

EFQ would like to thank CNPq for support through his doctor's degree scholarship.

7. References

A. G. Lee, E. S. G. S. and Khomami, B., 2002, A Study of Viscoelastic Free Surface Flows by the Finite Element Method: Hele-Shaw and Slot Coating Flows, "Journal of Non-Newtonian Fluid Mechanics", Vol. 108, pp. 327–362.

Bretherton, F. P., 1961, Viscous Fingering in Complex Fluids, "Journal of Fluid Mechanics", Vol. 10, pp. 166–188.

Brooks, A. N. and Hughes, T. J. R., 1982, Streamline Upwind Petrov-Galerkin Formulations for Convection Dominated Flows with Particular Emphasis on the Incompressible Navier-Stokes Equations, "Comput. Methods Appl. Mech. Eng.", Vol. 32, pp. 199–259.

Cox, B. G., 1962, On Driving a Viscous Fluid Out of a Tube, "Journal of Fluid Mechanics", Vol. 14, pp. 81–96.

D. Bonn, H. Kellay, M. B. M. B. A. and Meunier, J., 1995, Viscous Fingering in Complex Fluids, "Physica A", Vol. 220, pp. 60–73.

Fairbrother, F. and Stubbs, A. E., 1935, Studies in Electroendosmosis. Part IV. The Bubble-Tube Method of Measurements, "Journal of Chemical Society", Vol. 1, pp. 527–529.

Guenette, R. and Fortin, M., 1995, A New Mixed Finite Element Method for Computing Viscoelastic Flows, "Journal of Non-Newtonian Fluid Mechanics", Vol. 60, pp. 27–52.

Herrchen, M. and Ottinger, H. C., 1997, A Detailed Comparison of Various FENE dumbbell models, "Journal of Non-Newtonian Fluid Mechanics", Vol. 68, pp. 17–42.

Huzyak, P. C. and Koelling, K. W., 1997, The Penetration of a Long Bubble Through a Viscoelastic Fluid in a Tube, "Journal of Non-Newtonian Fluid Mechanics", Vol. 71, pp. 73–88.

R. B. Bird, R. C. A. and Hassager, O., 1987a, "Dynamics of Polymeric Liquids, Vol. 1: Fluid Mechanics", John Wiley & Sons, New York, USA, 650 p.

R. B. Bird, C. F. Curtiss, R. C. A. and Hassager, O., 1987b, "Dynamics of Polymeric Liquids, Vol. 2: Kinetic Theory", John Wiley & Sons, New York, USA, 650 p.

Ro, J. S. and Homsy, G. M., 1995, Viscoelastic Free Surface Flows: Thin Film Hydrodynamics of Hele-Shaw and Dip Coating Flows, "Journal of Non-Newtonian Fluid Mechanics", Vol. 57, pp. 203–225.

Taylor, G. I., 1961, Deposition of a Viscous Fluid on the Wall of a Tube, "Journal of Fluid Mechanics", Vol. 10, pp. 161–165.